

Multi-orbital Fulde-Ferrell-Larkin-Ovchinnikov State in SrTiO₃ Heterostructures

Yasuharu Nakamura¹ and Youichi Yanase^{1,2*}

¹Graduate School of Science and Technology, Niigata University, Niigata 950-2181, Japan

²Department of Physics, Niigata University, Niigata 950-2181, Japan

(Received August 11, 2014)

We study exotic superconducting states in SrTiO₃ heterostructures on the basis of the three-orbital model, which reproduces the band structure of two-dimensional electron gases. We show various Fulde-Ferrell-Larkin-Ovchinnikov (FFLO) states induced by the broken inversion symmetry and orbital degree of freedom. In particular, a novel orbital-dependent FFLO state is stabilized in a magnetic field along the [110]-axis. The field angle dependence of the FFLO state is clarified on the basis of the spin and orbital texture in the momentum space. It is shown that the orbital degree of freedom in Cooper pairs gives rise to in-plane anisotropy of the critical magnetic field. The carrier density dependence of the superconducting state is also discussed.

1. Introduction

Since the discovery of two-dimensional conducting electron gases at the interface between two band insulator perovskite oxides SrTiO₃/LaAlO₃,¹⁾ quantum phases in SrTiO₃ heterostructures have been explored extensively. Superconductivity has been found not only in the SrTiO₃/LaAlO₃ interface²⁾ but also on the SrTiO₃ surface induced by an electric double-layer transistor (EDLT).³⁾ Superconductivity also occurs in the SrTiO₃/LaTiO₃ interface⁴⁾ and δ -doped SrTiO₃.⁵⁾ Interestingly, these superconducting states are artificially tuned by the gate voltage.^{3,6-10)} The EDLT technique also realized electric-field-induced superconductivity in KTaO₃, MoS₂, ZrNCl, and La_{1-x}Sr_xCuO₄.⁶⁾ In this paper, we propose exotic superconducting states that appear in SrTiO₃ heterostructures.

Superconductivity induced by the condensate of Cooper pairs having a finite center-of-mass momentum was proposed by Fulde and Ferrell¹¹⁾ and by Larkin and Ovchinnikov¹²⁾ five decades ago,¹³⁾ although the standard BCS theory assumes a zero center-of-mass momentum in Cooper pairs.¹⁴⁾ Experimental searches for the Fulde-Ferrell-Larkin-Ovchinnikov (FFLO) state found the heavy-fermion superconductor CeCoIn₅,^{15,16)} some organic superconductors,¹⁷⁻²⁰⁾ and iron-based superconductors²¹⁻²³⁾ to be promising candidates. The FFLO states in population-imbalanced cold fermion gases²⁴⁾ and in nuclear matter²⁵⁾ have also attracted interest.

For the FFLO state rather than the BCS state to be stabilized, the spin polarization must be caused by something that breaks the time-reversal symmetry, such as an applied magnetic field or proximity to a ferromagnet.¹¹⁻¹³⁾ A magnetic field is most easily achieved, but it simultaneously leads to the orbital depairing effect and often destabilizes the FFLO state.^{26,27)} In the above candidate materials for the FFLO superconductor, the heavy and anisotropic effective mass of quasiparticles suppresses the orbital depairing effect and allows the FFLO state to be stabilized. On the other hand, the orbital depairing effect is completely suppressed when a magnetic field is applied parallel to the conducting plane of two-dimensional electron gases. Therefore, SrTiO₃ heterostruc-

tures are a valuable platform for realizing the FFLO state.

The artificial tuning of the superconducting state using the gate voltage^{3,6-10)} may enable a novel FFLO state to emerge. For instance, the lack of space inversion symmetry on the surface/interface allows an FFLO state beyond the paradigm of Fulde and Ferrell and of Larkin and Ovchinnikov. For clarity, we adopt the following classification of the FFLO state. The Fulde-Ferrell (FF) state is the single- Q condensate represented by the order parameter $\Delta(\mathbf{r}) = \Delta e^{i\mathbf{q}\mathbf{r}}$ in real space,¹¹⁾ whereas the Larkin-Ovchinnikov (LO) state is the double- Q state where $\Delta(\mathbf{r}) = \Delta(e^{i\mathbf{q}\mathbf{r}} + e^{-i\mathbf{q}\mathbf{r}})/2 = \Delta \cos(\mathbf{q}\mathbf{r})$.¹²⁾ While the phase of the order parameter shows spatial modulation in the FF state, the order parameter in the LO state acquires amplitude modulation. Furthermore, it has been shown that the triple- Q , quadruple- Q , and sextuple- Q states are stabilized when the Fermi surface has cylindrical symmetry.²⁸⁾

Recent theoretical studies on superconductivity lacking inversion symmetry, which is called noncentrosymmetric superconductivity,²⁹⁾ elucidated a “helical superconducting state” similar to the FF state.³⁰⁻³⁵⁾ Owing to the antisymmetric spin-orbit coupling appearing in noncentrosymmetric crystals,²⁹⁾ the helical state is stabilized in the low-magnetic-field region above H_{c1} , in contrast to the FFLO state which requires a high magnetic field close to the Pauli limit to be stabilized in centrosymmetric crystals. It has also been shown that an intermediate state between the FF and LO states, which we call the “complex stripe (CS) state”, emerges from the helical state.³⁴⁾ A helical state robust against spin polarization has been proposed for the SrTiO₃/LaAlO₃ interface³⁶⁾ in order to elucidate the coexistence of superconductivity and ferromagnetic order.³⁷⁻⁴¹⁾

Although these previous theories are based on single-band and single-orbital models, it has been shown that the orbital degree of freedom in t_{2g} electrons plays an important role in the magnetic response of superconducting SrTiO₃ heterostructures.⁴²⁾ Thus, a further novel FFLO state may be induced by the cooperation between the broken inversion symmetry and the orbital degree of freedom. Although the FFLO superconductivity in multi-band models has been investigated in recent studies⁴³⁻⁴⁵⁾ triggered by the observation of a paramagnetic depairing effect in iron-based superconductors,²¹⁻²³⁾ the orbital degree of freedom has not been taken into account.

*E-mail address: yanase@phys.sc.niigata-u.ac.jp

When we assume a pairing interaction on the band basis as in the literature,^{43–45} the momentum dependence of the orbital wave function in the band is neglected. On the other hand, it is naturally taken into account in the multi-orbital model that we adopt in this paper. Furthermore, the Rashba spin-orbit coupling, which plays an essential role in this study, is appropriately derived in the multi-orbital model,⁴⁶ although it is difficult to do so in multi-band models. Thus, the multi-orbital model is a reasonable starting point in this study. We show that the multi-orbital nature gives rise to an FFLO state beyond the multi-band models.

In this work, we investigate superconducting SrTiO₃ in a parallel magnetic field on the basis of the three-orbital model, which reproduces the band structure of two-dimensional electron gases, and examine the roles of the orbital degree of freedom and spin-orbit coupling. It is shown that the orbital degeneracy in t_{2g} -orbitals on the Ti ions markedly affects the FFLO state. In particular, we obtain the following results for the multi-orbital FFLO state, (1) a rich phase diagram involving the orbital-dependent complex stripe state, which has not been revealed for single-band models,^{30–35} and (2) highly anisotropic behaviors of the superconducting state with respect to the in-plane rotation of the magnetic field. We also investigate the evolution of the FFLO state by increasing the carrier density, which can be controlled by applying the gate voltage.^{3,6–10}

In Sect. 2, we introduce the three-orbital tight-binding model for SrTiO₃ heterostructures, and explain the linearized gap equation by which the superconducting instability is investigated. In Sect. 3.1, the in-plane anisotropy of the critical magnetic field is shown and attributed to the spin texture, which is affected by the orbital degeneracy. The FFLO states in magnetic fields parallel to the [100]-axis and [110]-axis are studied in Sects. 3.2 and 3.3, respectively. The in-plane field angle dependence of the superconducting state is illustrated in Sect. 3.4. The carrier density dependence of the FFLO states is discussed in Sect. 4. Finally in Sect. 5, we summarize the results and propose experimental searches for the various FFLO states in SrTiO₃ heterostructures.

2. Formulation

2.1 Three-orbital model for SrTiO₃ heterostructures

We adopt a three-orbital tight-binding model for t_{2g} -orbitals on Ti ions. As shown by experiments^{47–50} and electronic structure calculations,^{50–56} the conduction bands in SrTiO₃ heterostructures mainly consist of t_{2g} -orbitals. Although the electronic structure depends on the interface/surface termination, the band structure of two-dimensional electron gases is described by the one-body part of the Hamiltonian,

$$H_0 = H_{\text{kin}} + H_{\text{hyb}} + H_{\text{CEF}} + H_{\text{odd}} + H_{\text{LS}}, \quad (1)$$

$$H_{\text{kin}} = \sum_{\mathbf{k}} \sum_{m=1,2,3} \sum_{s=\uparrow,\downarrow} (\varepsilon_m(\mathbf{k}) - \mu) c_{\mathbf{k},ms}^\dagger c_{\mathbf{k},ms}, \quad (2)$$

$$H_{\text{hyb}} = \sum_{\mathbf{k}} \sum_{s=\uparrow,\downarrow} [V(\mathbf{k}) c_{\mathbf{k},1s}^\dagger c_{\mathbf{k},2s} + \text{h.c.}], \quad (3)$$

$$H_{\text{CEF}} = \Delta \sum_i n_{3i}, \quad (4)$$

$$H_{\text{odd}} = \sum_{\mathbf{k}} \sum_{s=\uparrow,\downarrow} [V_x(\mathbf{k}) c_{\mathbf{k},1s}^\dagger c_{\mathbf{k},3s} + V_y(\mathbf{k}) c_{\mathbf{k},2s}^\dagger c_{\mathbf{k},3s} + \text{h.c.}], \quad (5)$$

$$H_{\text{LS}} = \lambda \sum_i \mathbf{L}_i \cdot \mathbf{S}_i, \quad (6)$$

where $c_{\mathbf{k},ms}$ is the annihilation operator for an electron with momentum \mathbf{k} , orbital m , and spin s . Here, the (d_{yz} , d_{zx} , d_{xy})-orbitals are denoted by the orbital index $m = (1, 2, 3)$, respectively. The first term H_{kin} describes the kinetic energy of each orbital and includes the chemical potential μ . The second term H_{hyb} is the intersite hybridization term of d_{yz} - and d_{zx} -orbitals. The third term H_{CEF} introduces the crystal electric field with tetragonal symmetry.

Since the mirror symmetry with respect to the conducting plane is broken by the interface/surface, hybridization is allowed between the d_{xy} -orbital and (d_{yz} , d_{zx})-orbitals,^{56,57} which is represented by the odd-parity hybridization term H_{odd} . Thus, the broken inversion symmetry is introduced in our model. The Rashba spin-orbit coupling appears as an effective spin-orbit coupling arising from the odd-parity hybridization term H_{odd} and the LS coupling term H_{LS} .^{46,56,58} Although the Rashba spin-orbit coupling is often assumed phenomenologically in theoretical models,²⁹ it is microscopically derived in our model.

The following tight-binding forms are adopted in this paper.

$$\varepsilon_1(\mathbf{k}) = -2t_3 \cos k_x - 2t_2 \cos k_y, \quad (7)$$

$$\varepsilon_2(\mathbf{k}) = -2t_2 \cos k_x - 2t_3 \cos k_y, \quad (8)$$

$$\varepsilon_3(\mathbf{k}) = -2t_1(\cos k_x + \cos k_y) - 4t_4 \cos k_x \cos k_y, \quad (9)$$

$$V(\mathbf{k}) = 4t_5 \sin k_x \sin k_y, \quad (10)$$

$$V_x(\mathbf{k}) = 2it_{\text{odd}} \sin k_x, \quad (11)$$

$$V_y(\mathbf{k}) = 2it_{\text{odd}} \sin k_y. \quad (12)$$

The electronic structure of two-dimensional electron gases in the SrTiO₃/LaAlO₃ interface^{48,49,51–56} is reproduced by the parameter set $(t_1, t_2, t_3, t_4, t_5, t_{\text{odd}}, \lambda, \Delta) = (1, 1, 0.2, 0.4, 0.1, 0.1, 0.1, 2.45)$, where the unit of energy is chosen as $t_1 = 1$. A first-principles band structure calculation⁵⁵ obtained $t_1 \approx 300$ meV. In this paper, we mainly investigate a high two-dimensional carrier density of $n = 0.15 \approx 1 \times 10^{14} \text{ cm}^{-2}$, which has been realized in a gate-controlled SrTiO₃/LaAlO₃ interface⁹) and in a SrTiO₃ surface.³) We show the carrier density dependence of the superconducting state in Sect. 4 and demonstrate that unusual properties disappear in the lower carrier density region.

For the study of superconductivity, we assume attractive interactions in the s -wave channel,

$$H_I = U \sum_i \sum_m n_{i,m\uparrow} n_{i,m\downarrow} + U' \sum_i \sum_{m \neq m'} n_{i,m\uparrow} n_{i,m'\downarrow}, \quad (13)$$

where U and U' describe the intraorbital and interorbital attractive interactions, respectively. The s -wave symmetry of the superconductivity has been evidenced by both theory and experiment. A measurement of superfluid density showed the full excitation gap in the superconducting state.⁵⁹ Furthermore, it has been theoretically shown that the transition temperature of approximately 0.3 K and its nonmonotonic carrier density dependence in the SrTiO₃/LaAlO₃ interface are reproduced by the s -wave attractive interaction mediated by optical phonons.⁶⁰ The renormalization of the band structure observed by ARPES measurements has also been explained

by taking into account the electron-phonon coupling.⁵⁰⁾ Thus, *s*-wave superconductivity is likely to occur in SrTiO₃ heterostructures as well as in bulk SrTiO₃.⁶¹⁾ We assume $U = U'$ and choose U so that the transition temperature at zero magnetic field is $T_c = 0.001$. It has been confirmed that the following results are almost independent of U and the ratio U'/U as long as the reasonable condition $U'/U \leq 1$ is satisfied.⁶²⁾ We do not take into account the pairing interaction in the odd-parity channel, and thus the parity mixing in Cooper pairs is ignored. This simplification is also justified because the role of induced odd-parity Cooper pairs in FFLO superconductivity is negligible unless the amplitude of odd-parity Cooper pairs is comparable to that of even-parity Cooper pairs.^{63,64)} Although superconductivity induced by odd-parity Cooper pairs has been theoretically proposed,^{65,66)} we do not consider such unconventional Cooper pairing, which may be caused by the strong electron correlation.

The purpose of our study is to elucidate the spin-polarized FFLO superconducting states in the two-dimensional electron gases formed on SrTiO₃ heterostructures. Thus, we consider the Zeeman coupling term, which is induced by a magnetic field or by the coexisting ferromagnetic order,³⁶⁾

$$H_Z = - \sum_{\mathbf{k}} \sum_m \sum_{s,s'} \mu_B \mathbf{H} \cdot \boldsymbol{\sigma}_{ss'} c_{\mathbf{k},ms}^\dagger c_{\mathbf{k},ms'}, \quad (14)$$

where $\boldsymbol{\sigma}$ is the Pauli matrix and μ_B is the Bohr magneton. When we apply a magnetic field, superconductivity is destroyed through the orbital depairing effect as well as through the spin polarization induced by the Zeeman coupling term (paramagnetic depairing effect). However, the orbital depairing effect is negligible for a magnetic field parallel to two-dimensional electron gases, although it reduces the critical magnetic field along the [001]-axis to $H_{c2}^c \sim 0.1$ T, which is much smaller than the Pauli limit. The ferromagnetic moment coexisting with the superconductivity is parallel to the conducting plane,³⁸⁻⁴¹⁾ and thus the proximity effect gives rise to the effective magnetic field \mathbf{H} along the *ab*-plane. Thus, we assume a parallel magnetic field in the following sections and ignore the orbital depairing effect. The total Hamiltonian is given by $H = H_0 + H_1 + H_Z$.

2.2 Linearized gap equation

We determine the instability to the superconducting state by solving the linearized mean field gap equation formulated in the following manner. First, we diagonalize the one-body Hamiltonian $H_0 + H_Z$ using the unitary matrix

$$\hat{U}(\mathbf{k}) = \begin{pmatrix} u_{1\uparrow,1} & \cdots & u_{1\uparrow,6} \\ u_{2\uparrow,1} & \cdots & u_{2\uparrow,6} \\ \vdots & \ddots & \vdots \\ u_{3\downarrow,1} & \cdots & u_{3\downarrow,6} \end{pmatrix}. \quad (15)$$

Thereby, the basis changes as $C_{\mathbf{k}}^\dagger = \Gamma_{\mathbf{k}}^\dagger U^\dagger(\mathbf{k})$, where $C_{\mathbf{k}}^\dagger = (c_{\mathbf{k},1\uparrow}^\dagger, c_{\mathbf{k},2\uparrow}^\dagger, \dots, c_{\mathbf{k},3\downarrow}^\dagger)$ and $\Gamma_{\mathbf{k}}^\dagger = (\gamma_{\mathbf{k},1}^\dagger, \gamma_{\mathbf{k},2}^\dagger, \dots, \gamma_{\mathbf{k},6}^\dagger)$. By using the operators in the band basis, the one-body Hamiltonian is diagonalized as

$$H_0 + H_Z = \sum_{\mathbf{k}} \sum_{j=1}^6 E_j(\mathbf{k}) \gamma_{\mathbf{k},j}^\dagger \gamma_{\mathbf{k},j}, \quad (16)$$

where $E_j(\mathbf{k})$ is the energy of a quasiparticle and we take $E_i(\mathbf{k}) \geq E_j(\mathbf{k})$ for $i > j$. The Matsubara Green functions in the spin and orbital basis are obtained as[@]

$$G_{m's', ms}(\mathbf{k}, i\omega_l) = - \int_0^\beta d\tau e^{i\omega_l \tau} \langle c_{\mathbf{k},m's'}(\tau) c_{\mathbf{k},ms}^\dagger(0) \rangle, \quad (17)$$

$$= \sum_{j=1}^6 \frac{1}{i\omega_l - E_j(\mathbf{k})} u_{m's',j}(\mathbf{k}) u_{ms,j}^*(\mathbf{k}), \quad (18)$$

where ω_l is the Matsubara frequency.

The linearized gap equation is formulated by considering the divergence of the T-matrix, which is defined as

$$\hat{T}(\mathbf{q}) = \hat{T}_0(\mathbf{q}) - \hat{T}(\mathbf{q}) \hat{H}_1 \hat{T}_0(\mathbf{q}). \quad (19)$$

The wave vector \mathbf{q} represents the center-of-mass momentum of Cooper pairs. The matrix element of the irreducible T-matrix $\hat{T}_0(\mathbf{q})$ is obtained as

$$T_0^{(mn, m'n')}(\mathbf{q}) = T \sum_{\omega_l} \sum_{\mathbf{k}} [G_{m'\uparrow, m\uparrow}(\mathbf{q}/2 + \mathbf{k}, i\omega_l) G_{n\downarrow, n\downarrow}(\mathbf{q}/2 - \mathbf{k}, -i\omega_l) - G_{n'\downarrow, m\uparrow}(\mathbf{q}/2 + \mathbf{k}, i\omega_l) G_{m'\uparrow, n\downarrow}(\mathbf{q}/2 - \mathbf{k}, -i\omega_l)], \quad (20)$$

where T is the temperature. When we represent the T-matrix using the basis $(mn) = (11, 12, 13, 21, 22, 23, 31, 32, 33)$, the interaction term is represented by the 9×9 diagonal matrix $\hat{H}_1 = (U_m \delta_{mn})$ with $U_m = U$ for $m = 1, 5, 9$ and $U_m = U'$ for others. The superconducting transition occurs when the maximum eigenvalue λ_{\max} of the matrix, $-\hat{H}_1 \hat{T}_0(\mathbf{q})$, is unity. The order parameter in the orbital basis is obtained from the eigenvector (ψ_{mn}) , which is proportional to $\Delta_{mn} = -g \sum_{\mathbf{k}} \langle c_{\mathbf{q}/2+\mathbf{k}, m\uparrow} c_{\mathbf{q}/2-\mathbf{k}, n\downarrow} \rangle$ with $g = U$ for $m = n$ and $g = U'$ for $m \neq n$. Thus, the superconducting state below the transition temperature $T_c(H)$ is determined by the linearized gap equation, although the full solution of the Bogoliubov-de Gennes equation is required for studying the superconducting state at low temperatures.

The superconducting transition is induced by the quasi-long-range order in two-dimensional systems and described by the Berezinskii-Kosterlitz-Thouless (BKT) transition.^{67,68)} Although even the quasi-long-range order of FFLO superconductivity is suppressed in isotropic two-dimensional systems, the anisotropy in the Fermi surface allows the quasi-long-range order.⁶⁹⁾ Indeed, critical behaviors of the BKT transition have been observed in the SrTiO₃/LaAlO₃ interface.^{2,7,70)} The BKT transition temperature is roughly obtained using the following equation:⁶⁸⁾

$$T_{\text{BKT}} = \frac{\pi}{2m^*} \rho(T_{\text{BKT}}), \quad (21)$$

where $\rho(T)$ is the superfluid density. Because of the large superfluid density and small transition temperature of SrTiO₃ heterostructures, the transition temperature obtained on the basis of mean field theory (T_c) almost coincides with the BKT transition temperature (T_{BKT}),²⁾ as $1 - T_{\text{BKT}}/T_c \ll 1$. Thus, the superconductivity in SrTiO₃ heterostructures is approximately described on the basis of mean field theory, although the long-range order obtained using mean field theory is interpreted as a quasi-long-range order at finite temperatures.

2.3 Classification of FFLO states

For clarity, we classify various FFLO states, which will appear in the following sections. Although the FFLO states have been classified into the single- Q FF state¹¹⁾ and double- Q LO state,¹²⁾ the so-called helical state can emerge in non-centrosymmetric superconductors.^{30–35)} The order parameter of the helical state is formally the same as that of the FF state, but the magnitude of the center-of-mass momentum, $|\mathbf{q}| \sim (\alpha/E_F) \cdot (\mu_B H/T_c) \cdot \xi^{-1}$, is much smaller than that in the FF state, $|\mathbf{q}| \sim \xi^{-1}$, where ξ is the coherence length. The helical state is stabilized by the asymmetric deformation of Fermi surfaces arising from the antisymmetric spin-orbit coupling and magnetic field.²⁹⁾ Therefore, the magnitude $|\mathbf{q}|$ is proportional to α and H . Thus, long-period spatial modulation characterizes the helical state. Indeed, the crossover from the helical state to the FF state occurs by increasing the magnetic field,⁶³⁾ and we differentiate these two states by looking at the magnitude of \mathbf{q} . Above the crossover field, the CS state where $\Delta(\mathbf{r}) = \Delta(e^{i\mathbf{q}\mathbf{r}} + \delta e^{-i\mathbf{q}\mathbf{r}})/2 \neq \Delta \cos(\mathbf{q}\mathbf{r})$ may be stabilized in the low-temperature region.³⁴⁾ Below, we will show that a novel two-component CS state due to the orbital degree of freedom is stabilized in SrTiO₃ heterostructures (see Sect. 3.3).

3. FFLO superconductivity

As we find that the superconducting state markedly depends on the direction of the magnetic field, we first show the anisotropic paramagnetic depairing effect in Sect. 3.1. Then, we show the FFLO superconducting states for $\mathbf{H} \parallel [100]$ and $\mathbf{H} \parallel [110]$ in Sects. 3.2 and 3.3, respectively. The field angle dependence of the superconducting state for $\mathbf{H} \parallel (\cos \theta, \sin \theta, 0)$ is discussed in Sect. 3.4.

3.1 In-plane anisotropy of paramagnetic depairing effect

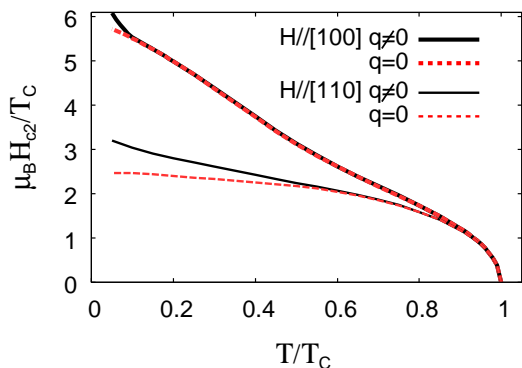


Fig. 1. (Color online) Critical magnetic fields of the BCS state (red dashed lines) and FFLO state (black solid lines). Thick and thin lines show the normalized critical magnetic fields $\mu_B H_{c2}/T_c$ along the [100]- and [110]-axes, respectively. We assume the carrier density $n = 0.15 \approx 1 \times 10^{14} \text{ cm}^{-2}$ throughout Sect. 3.

First, we show the anisotropy of the paramagnetic depairing effect, which arises from the orbital degeneracy in the electronic structure. We also study the thermodynamical stability of the FFLO state by comparing the critical magnetic fields of the BCS state and FFLO state. Figure 1 shows that the critical magnetic field is enhanced by allowing the Cooper

pairs to have a finite center-of-mass momentum. However, for $\mathbf{H} \parallel [100]$, the enhancement is negligible and is much smaller than the effect of canonical FFLO superconductivity on the critical magnetic field.¹³⁾ On the other hand, the critical magnetic field along the [110]-axis is considerably enhanced. Since the critical magnetic field for $\mathbf{H} \parallel [110]$ is smaller than that for $\mathbf{H} \parallel [100]$, a larger paramagnetic depairing effect is indicated for the former.

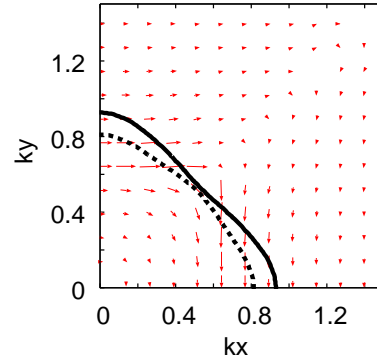


Fig. 2. (Color online) Spin texture in the 1st band. Arrows show the g-vector $\mathbf{g}_1(\mathbf{k})$ defined in Eq. (22). Solid and dashed lines show the Fermi surfaces split by spin-orbit coupling.

We explain the large anisotropy of the paramagnetic depairing effect by illustrating the spin texture of spin-split bands. The spin degeneracy in the band structure is lifted by the spin-orbit coupling in a noncentrosymmetric metal.²⁹⁾ The momentum-dependent spin polarization is described by the “g-vector”, which is defined for the l th band as^{42,58)}

$$\mathbf{g}_l(\mathbf{k}) = (E_{2l}(\mathbf{k}) - E_{2l-1}(\mathbf{k})) \tilde{\mathbf{S}}_{2l}^{\text{av}}(\mathbf{k}). \quad (22)$$

The spin polarization axis $\tilde{\mathbf{S}}_{2l}^{\text{av}}(\mathbf{k}) = \mathbf{S}_{2l}^{\text{av}}(\mathbf{k})/|\mathbf{S}_{2l}^{\text{av}}(\mathbf{k})|$ is obtained by calculating the average spin $\mathbf{S}_{2l}^{\text{av}}(\mathbf{k}) = \langle \sum_m \sum_{ss'} \sigma_{ss'} c_{\mathbf{k},ms}^\dagger c_{\mathbf{k},ms'} \rangle_{2l}$ for each momentum \mathbf{k} . The arrows in Fig. 2 show the g-vector of the 1st band whose spin-split Fermi surfaces are shown by the solid and dashed lines. We see that the g-vector is almost perpendicular to the [100]-axis in half of the Brillouin zone, $|k_x| > |k_y|$, where the 1st band mainly consists of the d_{yz} -orbital. As shown in the literature,²⁹⁾ Cooper pairs are robust against the paramagnetic depairing effect when the spin polarization axis is perpendicular to the magnetic field. Thus, the quasi-one-dimensional superconducting state mainly induced by the d_{yz} -orbital substantially avoids the paramagnetic depairing effect for $\mathbf{H} \parallel [100]$.⁴²⁾ Indeed, a large critical magnetic field beyond the Pauli limit has been observed in the SrTiO₃/LaAlO₃ interface.⁹⁾ On the other hand, we see that the spin polarization axis is not perpendicular to the [110]-axis in the entire Brillouin zone except for a tiny region near $k_x = k_y$. Therefore, the large paramagnetic depairing effect suppresses the BCS state for $\mathbf{H} \parallel [110]$, and it is partly avoided in the FFLO state.

The large anisotropy discussed above is attributed to the orbital degree of freedom in the t_{2g} electron system. Indeed, the spin texture shown in Fig. 2 is typical for an orbitally degenerate noncentrosymmetric metal. When the crystal electric field is sufficiently large so that the orbital degree of freedom is quenched, an often assumed Rashba-type antisymmetric spin-

orbit coupling [$\mathbf{g}_l(\mathbf{k}) \propto (\sin k_y, -\sin k_x, 0)$] is obtained.⁵⁸⁾ On the other hand, in orbitally degenerate systems, the \mathbf{g} -vector dramatically changes direction near the symmetric axis in the Brillouin zone,⁵⁸⁾ as clearly shown in Fig. 2. Thus, the characteristic spin texture in the multi-orbital systems causes the anisotropic behaviors of superconductivity with respect to the magnetic field. In the following subsections, we show that the FFLO states in SrTiO₃ heterostructures depend on the in-plane direction of the magnetic field.

3.2 Nonmonotonic evolution of FFLO state in $\mathbf{H} \parallel [100]$

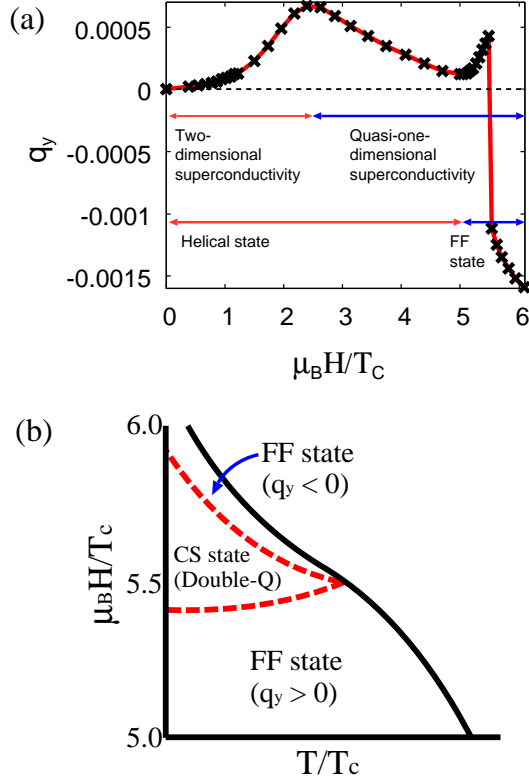


Fig. 3. (Color online) (a) center-of-mass momentum in Cooper pairs at $T = T_c(H)$ as a function of the magnetic field along the [100]-axis. As $\mathbf{q} = q_y \hat{y}$, we plot q_y . The crossover in the superconducting state is described (see the text for details). (b) Schematic phase diagram in the high-magnetic-field region. Multiple superconducting transitions are illustrated by red dashed lines.

The superconducting state shows several crossovers and the FFLO state nonmonotonically changes with increasing magnetic field along the [100]-axis. The antisymmetric spin-orbit coupling arising from the interfacial mirror-symmetry breaking is of the Rashba type,⁷¹⁾ and thus the Cooper pairs acquire a center-of-mass momentum perpendicular to the magnetic field.²⁹⁾ Indeed, we obtain $\mathbf{q} \parallel [010]$ unless $\mathbf{H} = 0$. Figure 3(a) shows the [010]-component q_y as a function of the magnetic field. We see a peak at approximately $\mu_B H/T_c = 2.4$, although $|q_y|$ monotonically increases with the magnetic field in single-band models.⁶³⁾ The peak is associated with the dimensional crossover of the superconducting state.⁴²⁾ The superconductivity is mainly induced by the degenerate (d_{yz} , d_{zx})-orbitals in the low-magnetic-field region, and it changes to the quasi-one-dimensional superconducting state induced by the d_{yz} -orbital at approximately $\mu_B H/T_c = 2.4$. Since the

paramagnetic depairing effect is suppressed in the latter, as we discussed in Sect. 3.1, the center-of-mass momentum in Cooper pairs is decreased with increasing magnetic field for $2.4 < \mu_B H/T_c < 5$.

The superconducting state shows another crossover from the helical state to the FF state at approximately $\mu_B H/T_c = 5$, as indicated by the second increase in q_y above $\mu_B H/T_c > 5$. Then, the sign of q_y suddenly changes at $\mu_B H/T_c = 5.5$. Because the two momenta are degenerate at $\mu_B H/T_c = 5.5$, the multiple superconducting phases appear, as illustrated in Fig. 3(b). Here, it is assumed that the Cooper pair condensates for both momenta $q_y = q_+ \sim +0.0005$ and $q_y = q_- \sim -0.0011$ coexist below T_c as in the single-band model.³⁴⁾ The superconducting state shows a phase transition from the single- Q FF state with $q_y > 0$ to the double- Q state, and it again changes to the single- Q FF state with $q_y < 0$ with increasing magnetic field.

The order parameter in the double- Q state is described as

$$\Delta_{mn}(\mathbf{r}) = \Delta_{mn}^{(+)} e^{iq_+ y} + \Delta_{mn}^{(-)} e^{iq_- y}. \quad (23)$$

Since $|q_+| \neq |q_-|$, both the amplitude and phase of the order parameter are spatially inhomogeneous as in the CS state. As the sign change of q_y does not occur in single-orbital models,^{33,34,63)} the multiple superconducting transitions illustrated in Fig. 3(b) are attributed to the orbital degree of freedom in t_{2g} electron systems.

3.3 Orbital-dependent FFLO state in $\mathbf{H} \parallel [110]$

Next, we investigate the FFLO state in a magnetic field along the [110]-axis. Figure 4 shows the marked increase in the center-of-mass momentum in Cooper pairs above the magnetic field $\mu_B H/T_c > 1.7$. Similar behavior has been obtained for single-band models for noncentrosymmetric superconductors.⁶³⁾ It indicates the crossover from the helical state to the FF state. However, the superconducting state in the high-magnetic-field region is distinct from the conventional FF state, as we will show below.

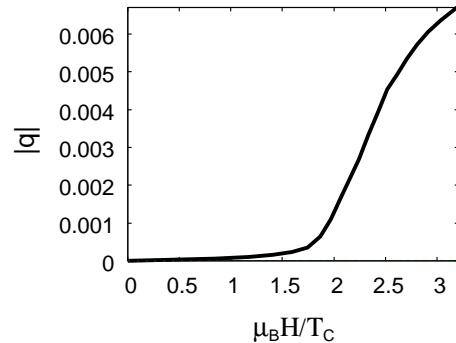


Fig. 4. Magnitude of center-of-mass momentum $|q|$ at $T = T_c(H)$ as a function of the magnetic field along the [110]-axis.

Figure 5 shows the center-of-mass momentum $\mathbf{q} = (q_x, q_y)$ in the two-dimensional momentum space for various magnetic fields. Although the isotropic Rashba superconductor acquires a center-of-mass momentum perpendicular to the in-plane magnetic field, namely, $\mathbf{q} \parallel [1\bar{1}0]$ in this case, we see a deviation of \mathbf{q} from the symmetric $[1\bar{1}0]$ -axis at high magnetic fields, $\mu_B H/T_c > 2.3$. The deviation is caused by the

quasi-one-dimensional nature of the Fermi surface, which favors the FFLO state with $\mathbf{q} \parallel [100]$ or $\mathbf{q} \parallel [010]$. The high-field FFLO state is determined by the competition between the Rashba spin-orbit coupling and the anisotropy in Fermi surfaces, and the center-of-mass momentum is generally represented as $\mathbf{q}_{1,2} = \mathbf{q}_\perp \pm \mathbf{q}_\parallel$. Here, we decomposed \mathbf{q}_1 and \mathbf{q}_2 into $\mathbf{q}_\perp \parallel [1\bar{1}0]$ and $\mathbf{q}_\parallel \parallel [110]$.

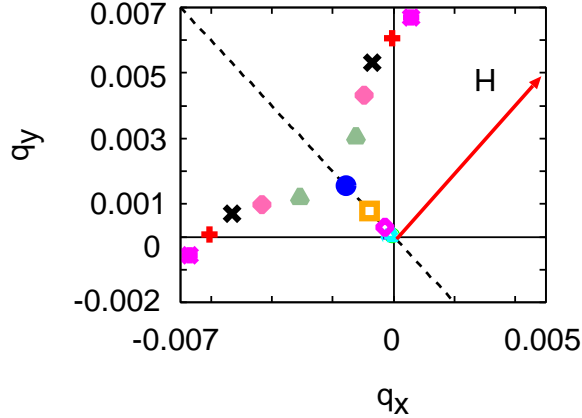


Fig. 5. (Color online) Center-of-mass momentum of Cooper pairs for various magnetic fields along the $[110]$ -axis. Each mark is obtained at a magnetic field and temperature represented in Fig. 6. The superconducting state is described by the two-component order parameters with respect to the center-of-mass momentum in the high-magnetic-field region.

Because of the mirror symmetry along the $[110]$ -axis, the superconducting state has twofold degeneracy with respect to the center-of-mass momentum, \mathbf{q}_1 and \mathbf{q}_2 . Thus, the superconducting state is described by the two-component order parameters $\boldsymbol{\eta} = (\eta_1, \eta_2)$, where η_1 corresponds to \mathbf{q}_1 and η_2 corresponds to \mathbf{q}_2 . The Ginzburg-Landau free energy is described as

$$F = -\alpha_0 \left(1 - \frac{T}{T_c(H)}\right) |\boldsymbol{\eta}|^2 + \frac{\beta}{2} |\boldsymbol{\eta}|^4 + \gamma |\eta_1|^2 |\eta_2|^2 + \kappa_1 (|D_{\bar{x}} \eta_1|^2 + |D_{\bar{x}'} \eta_2|^2) + \kappa_2 (|D_{\bar{y}} \eta_1|^2 + |D_{\bar{y}'} \eta_2|^2), \quad (24)$$

where $D_a = -i\partial_a + 2eA_a$ is a covariant derivative. Note that the principal axis of gradient terms is different between the two-component order parameters, as $(\bar{x}, \bar{y}) \neq (\bar{x}', \bar{y}')$. When the magnetic field is precisely applied to the ab -plane, the gradient terms do not play any role. Then, the double- Q state, where $\boldsymbol{\eta} \propto (1, e^{i\theta})$, is stable when $\gamma < 0$. On the other hand, the single- Q state, where $\boldsymbol{\eta} \propto (0, 1)$ or $\boldsymbol{\eta} \propto (1, 0)$, is stable otherwise.

The order parameter in the orbital basis is represented by $\boldsymbol{\eta}$ as

$$\Delta_{mn}(\mathbf{r}) = \eta_1 \Delta_{mn}^{(1)} e^{i\mathbf{q}_1 \cdot \mathbf{r}} + \eta_2 \Delta_{mn}^{(2)} e^{i\mathbf{q}_2 \cdot \mathbf{r}}, \quad (25)$$

$$= e^{i\mathbf{q}_\perp \cdot \mathbf{r}} \left[\eta_1 \Delta_{mn}^{(1)} e^{i\mathbf{q}_\parallel \cdot \mathbf{r}} + \eta_2 \Delta_{mn}^{(2)} e^{-i\mathbf{q}_\parallel \cdot \mathbf{r}} \right], \quad (26)$$

where $\Delta_{mn}^{(1)}$ and $\Delta_{mn}^{(2)}$ are obtained by the linearized gap equation for $\mathbf{q} = \mathbf{q}_1$ and $\mathbf{q} = \mathbf{q}_2$, respectively. For both momenta, the dominant components are $\Delta_{11}^{(1,2)}$ and $\Delta_{22}^{(1,2)}$, which describe the intra-orbital Cooper pairs formed by the d_{yz} - and d_{zx} -orbitals, respectively. We find that $|\Delta_{11}^{(1)}| = |\Delta_{22}^{(2)}| < |\Delta_{11}^{(2)}| = |\Delta_{22}^{(1)}|$, because the d_{yz} -orbital (d_{zx} -orbital) favors the FFLO

state with $\mathbf{q} \parallel [100]$ ($\mathbf{q} \parallel [010]$). Thus, the Cooper pairs in the single- Q state are ‘‘orbital-polarized’’.

On the other hand, the order parameter in the double- Q state is described as

$$\Delta_{11}(\mathbf{r}) = \Delta e^{i\mathbf{q}_\perp \cdot \mathbf{r}} \left[\delta e^{i\mathbf{q}_\parallel \cdot \mathbf{r}} + e^{-i\mathbf{q}_\parallel \cdot \mathbf{r}} \right], \quad (27)$$

$$\Delta_{22}(\mathbf{r}) = \Delta e^{i\mathbf{q}_\perp \cdot \mathbf{r}} \left[e^{i\mathbf{q}_\parallel \cdot \mathbf{r}} + \delta e^{-i\mathbf{q}_\parallel \cdot \mathbf{r}} \right], \quad (28)$$

where $\Delta = |\Delta_{11}^{(2)}| = |\Delta_{22}^{(1)}|$, and $\delta < 1$. For instance, we obtain $\delta = 0.88$ at $\mu_B H/T_c = 3.2$. Equations (27) and (28) are similar to the order parameter in the CS state, but they acquire a phase oscillation $e^{i\mathbf{q}_\perp \cdot \mathbf{r}}$. Furthermore, the average center-of-mass momentum in Cooper pairs depends on the orbital: it is $\mathbf{q}_\perp - \frac{1-\delta^2}{1+\delta^2} \mathbf{q}_\parallel$ for the d_{yz} -orbital and $\mathbf{q}_\perp + \frac{1-\delta^2}{1+\delta^2} \mathbf{q}_\parallel$ for the d_{zx} -orbital. Thus, we call the double- Q state the ‘‘orbital-dependent complex stripe (ODCS) state’’. An analogous ‘‘layer-dependent complex stripe state’’ has been proposed for multilayer superconductors affected by spin-orbit coupling.⁷²⁾

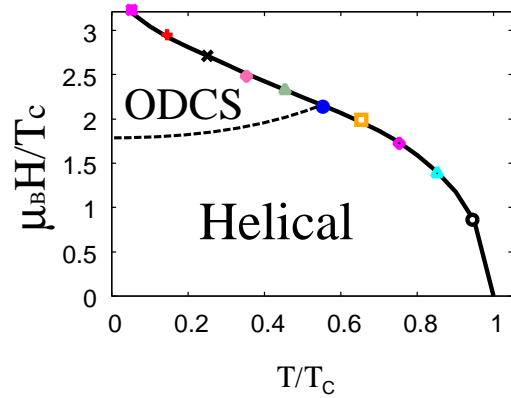


Fig. 6. (Color online) Phase diagram for $H \parallel [110]$. The solid line is the critical magnetic field obtained by our calculation, and the marks correspond to those in Fig. 5. A second-order phase transition line is schematically drawn by the dashed line. The ODCS state and helical state are stabilized in the high- and low-magnetic-field regions, respectively.

Because the orbital polarization in Cooper pairs costs finite energy, it is expected that the double- Q state is more stable than the single- Q state. Since the superconducting gap in the single- Q state is anisotropic in the momentum space, the single- Q state gains less condensation energy than the double- Q state. Thus, we assume $\gamma < 0$ and draw the schematic phase diagram in Fig. 6. The helical state is stabilized in the low-magnetic-field region, while the ODCS state is stable in the high-magnetic-field region. The continuous second-order phase transition occurs in the superconducting state, as illustrated by the dashed line, where \mathbf{q}_\parallel grows with increasing magnetic field.

The Ginzburg-Landau free energy in Eq. (24) conserves the $U(1) \times U(1)$ symmetry in the order parameter manifold. Therefore, the fractional vortex can emerge when the magnetic field is slightly tilted from the ab -plane. When the vortex cores of the η_1 component are shifted from those of the η_2 component, as favored for $-\beta < \gamma < 0$, a fractional vortex lattice is formed. The fractional vortex lattice has been topologically identified to be a skyrmion lattice of superconductivity.⁷³⁾

3.4 Field angle dependence

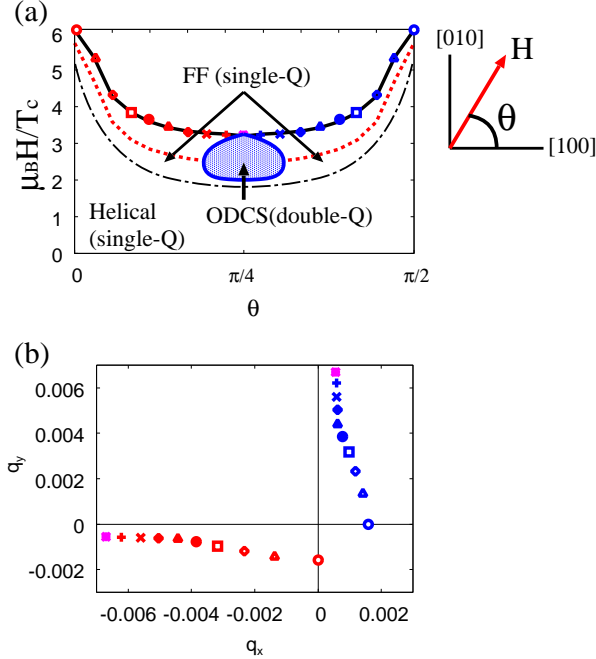


Fig. 7. (Color online) (a) The solid line shows the critical magnetic field at $T/T_c = 0.05$ as a function of θ , the angle of the in-plane magnetic field $\mathbf{H} = H(\cos \theta, \sin \theta, 0)$. The red dashed line is the critical field of the BCS state. We also show the crossover line between the helical state and the FF state (black dash-dotted line). The ODCS phase is schematically drawn by the shaded area. The double- Q CS state in Fig. 3(b) is not shown in this figure. (b) Cooper pair momentum $\mathbf{q} = (q_x, q_y)$ at $T/T_c = 0.05$ and $H = H_c2(T)$ for various magnetic field directions from $\theta = 0$ to $\theta = \pi/2$. Marks in Fig. 7(b) correspond to those in Fig. 7(a). For example, the open blue circle is obtained for $\theta = \pi/2$.

As we have discussed in Sects. 3.1-3.3, the paramagnetic depairing effect and the resulting FFLO state are markedly different between $\mathbf{H} \parallel [100]$ and $\mathbf{H} \parallel [110]$ because of the orbital degree of freedom in the t_{2g} electrons. Here, we clarify the field angle dependence of the superconducting state for $\mathbf{H} \parallel (\cos \theta, \sin \theta, 0)$.

Figure 7(a) shows the field angle dependence of the critical magnetic field. As we showed in Sect. 3.1, the critical magnetic field is enhanced near $\theta = 0$ and $\theta = \pi/2$, while it is insensitive to θ at around $\theta = \pi/4$. Thus, an experimental observation of the enhancement of the critical magnetic field at around $\theta = 0$ may indicate the orbital degree of freedom which plays an important role on the superconductivity in SrTiO₃ heterostructures.

When the magnetic field is slightly tilted from the [110]-axis, the degeneracy with respect to the center-of-mass momentum $\mathbf{q} = \mathbf{q}_1$ and $\mathbf{q} = \mathbf{q}_2$ is lifted. Therefore, the single- Q FF state is stable just below the critical magnetic field. However, the ODCS state is stabilized by decreasing the magnetic field when the field angle is close to $\theta = \pi/4$. A schematic phase diagram is drawn in Fig. 7(a). The FF state continuously changes to the helical state with decreasing magnetic field, as we discussed earlier.

Figure 7(b) shows the field angle dependence of the Cooper pair momentum. For $\mathbf{H} \parallel [100]$ and $[010]$, the momentum \mathbf{q} is perpendicular to the magnetic field, and the magnitude

$|q|$ is small because the paramagnetic depairing effect is suppressed. The magnitude grows with the tilting of the magnetic field to the [110]-axis. The center-of-mass momentum of the Cooper pairs markedly changes through $\theta = \pi/4$, where two momenta $\mathbf{q} = \mathbf{q}_1$ and $\mathbf{q} = \mathbf{q}_2$ are degenerate.

4. Carrier Density Dependence of FFLO State

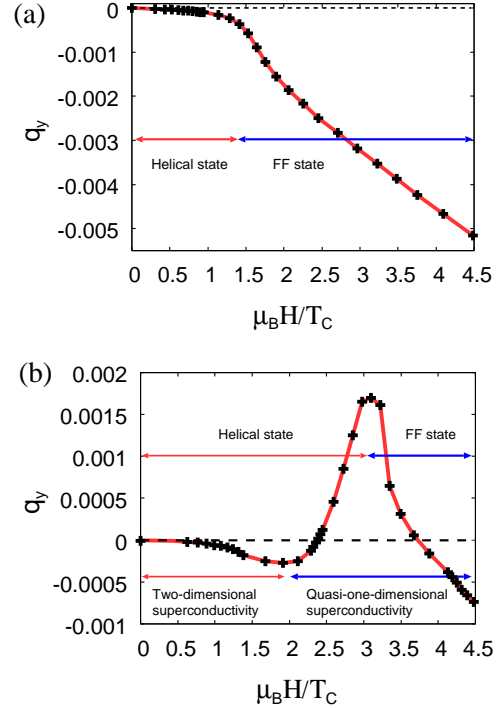


Fig. 8. (Color online) center-of-mass momentum in Cooper pairs at $T = T_c(H)$ as a function of the magnetic field along the [100]-axis. We assume carrier densities (a) $n = 0.05 \approx 3.5 \times 10^{13} \text{ cm}^{-2}$ and (b) $n = 0.1 \approx 7 \times 10^{13} \text{ cm}^{-2}$. We plot q_y as in Fig. 3(a).

While we clarified the unconventional FFLO states in the high-carrier-density region with $n = 0.15 \approx 1 \times 10^{14} \text{ cm}^{-2}$, here, we show that they disappear in the low-carrier-density region. It has been shown that the superconducting state changes with increasing carrier density from the d_{xy} -orbital-induced superconductivity to that induced by d_{yz}/d_{zx} -orbitals.⁴²⁾ For our choice of parameters, the crossover occurs at around $n = 0.07 \approx 5 \times 10^{13} \text{ cm}^{-2}$. This crossover density is larger than the experimentally observed value of $n \approx 2 \times 10^{13} \text{ cm}^{-2}$,⁴⁸⁾ but they are in reasonable agreement with each other. Below the crossover density, the orbital degree of freedom is almost quenched, and thus the unusual properties of FFLO superconductivity discussed in Sect. 3 do not appear. Indeed, the Cooper pair momentum shows conventional growth with the magnetic field [Fig. 8(a)]. For $n = 0.05 \approx 3.5 \times 10^{13} \text{ cm}^{-2}$, the superconducting state shows a single crossover from the helical state to the FF state as in single-band models.⁶³⁾ Since the paramagnetic depairing effect is not suppressed as much as in the quasi-one-dimensional superconducting state for $n = 0.15 \approx 1 \times 10^{14} \text{ cm}^{-2}$, the magnitude of the Cooper pair momentum is much larger than that in the high-carrier-density region [compare Fig. 8(a) with Fig. 3(a)]. We confirmed that the Cooper pair momentum is perpendicular to the magnetic

field even for $\mathbf{H} \parallel [110]$. Thus, the ODCS state is not stabilized at $n = 0.05 \simeq 3.5 \times 10^{13} \text{ cm}^{-2}$.

Near the crossover carrier density, namely, $n = 0.1 \simeq 7 \times 10^{13} \text{ cm}^{-2}$, the center-of-mass momentum in Cooper pairs changes sign twice, corresponding to the two crossovers discussed in Sect. 3.2. q_y is negative in the two-dimensional superconducting state at low magnetic fields, but it is positive in the quasi-one-dimensional superconducting state in the intermediate magnetic field region. It again changes sign at $\mu_B H/T_c \simeq 3.7$, where the helical state changes to the FF state. Thus, the nonmonotonic magnetic field dependence appears in the center-of-mass momentum of Cooper pairs. However, the sudden change in q_y does not occur in contrast to that shown in Fig. 3(a). Therefore, the double- Q CS state is not stabilized at least near $T = T_c(H)$. When we apply the magnetic field along the $[110]$ -axis, the ODCS state is stabilized, but the critical temperature of the ODCS state ($T_{\text{ODCS}}/T_c \sim 0.1$) is much smaller than that in the high-carrier-density region $n = 0.15 \simeq 1 \times 10^{14} \text{ cm}^{-2}$ ($T_{\text{ODCS}}/T_c \sim 0.5$). These results show that unusual FFLO states appear in SrTiO₃ heterostructures in the high-carrier-density region above the crossover density.

5. Summary and Discussion

We have investigated the multi-orbital FFLO superconductivity in two-dimensional electron gases on SrTiO₃ heterostructures. Owing to the broken inversion symmetry at the interface/surface, Cooper pairs acquire a finite center-of-mass momentum in a magnetic field parallel to the two-dimensional conducting plane. It has been demonstrated that unconventional FFLO states emerge in the high-carrier-density region owing to the orbital degree of freedom in t_{2g} electrons.

For $\mathbf{H} \parallel [100]$, the Cooper pair momentum shows a nonmonotonic magnetic field dependence indicating the crossover in the superconducting state. Indeed, the magnetic field changes the superconducting state from the two-dimensional helical state to the quasi-one-dimensional helical state, and a higher magnetic field stabilizes the quasi-one-dimensional FF state. Near the crossover from the helical state to the FF state, the Cooper pair momentum discontinuously changes, and the double- Q CS state is stabilized below T_c .

For $\mathbf{H} \parallel [110]$, the double- Q ODCS state is stabilized in the high-magnetic-field region. Therein, Cooper pairs formed by the d_{yz} -orbital and those formed by the d_{zx} -orbital have inequivalent center-of-mass momenta. These behaviors have not been shown in single-band models, and they are indeed attributed to the orbital degeneracy between the (d_{yz} , d_{zx})-orbitals. Thus, the ODCS state is a novel FFLO state in the multi-orbital system.

The unusual properties of the FFLO state disappear in the low-carrier-density region where the superconductivity is mainly induced by the single d_{xy} -orbital. Thus, a high carrier density is needed to stabilize the multi-orbital FFLO state studied in this paper. Combining our results with the experimental observation,⁴⁸⁾ we expect that SrTiO₃ heterostructures are in the high-carrier-density region when $n > 2 \times 10^{13} \text{ cm}^{-2}$. Two-dimensional electron gases with high carrier densities beyond $n = 1 \times 10^{14} \text{ cm}^{-2}$ have already been realized.^{3,6)}

Experimental studies of the superconducting state in a high magnetic field or in the ferromagnetic state are desired to clarify the FFLO state in SrTiO₃ heterostructures. We showed that

large in-plane anisotropy in the critical magnetic field will be evidence of the multi-orbital superconducting state. More direct observation of the FFLO state using scanning tunneling microscope (STM) and other techniques is of course desired. We hope that our proposal will be verified.

Finally, we discuss two ingredients that are not taken into account in our model. One is the subband structure. According to the band structure calculations,^{50–56)} several d_{xy} -orbital-derived subbands cross the Fermi level. On the other hand, the d_{yz}/d_{zx} -orbitals are quantized in the $[001]$ -axis direction because of their light effective mass. The subband structure in the d_{yz}/d_{zx} -orbitals is negligible, and thus the single-layer model adopted in this work is justified. Although the d_{xy} -orbital-derived subbands reduce the carrier density in the d_{yz}/d_{zx} -orbital-derived band, our results in the high-carrier-density region are not altered as long as a substantial part of carriers has a d_{yz}/d_{zx} -orbital property. The other ingredient neglected so far is the disorder. Although we investigated the superconducting state in the clean limit, the SrTiO₃ heterostructures indeed contain substantial disorder.^{3,8)} The disorder may alter our results for the multi-orbital FFLO state because it smears out the orbital character of the band. Furthermore, it has been shown that the disorder destabilizes the FFLO state,¹³⁾ although the helical state is not completely eliminated.²⁹⁾ Therefore, it is desirable to take into account the disorder for a comparison with experimental results. We leave this issue for a future study. It is also desirable to fabricate (at least locally) clean SrTiO₃ heterostructures.

Acknowledgements

The authors are grateful to T. Nojima and K. Ueno for fruitful discussions. This work was supported by a ‘‘Topological Quantum Phenomena’’ (No. 25103711) Grant-in Aid for Scientific Research on Innovative Areas from MEXT, Japan, and by a JSPS KAKENHI (No. 24740230). Y. N. was supported by a JSPS Fellowship for Young Scientists. Part of the numerical computation in this work was carried out at the Yukawa Institute Computer Facility.

- 1) A. Ohtomo and H. Y. Hwang, *Nature* **427**, 423 (2004).
- 2) N. Reyren, S. Thiel, A. D. Caviglia, L. Fitting Kourkoutis, G. Hammerl, C. Richter, C. W. Schneider, T. Kopp, A.-S. Rüetschi, D. Jaccard, M. Gabay, D. A. Muller, J.-M. Triscone, and J. Mannhart, *Science* **317**, 1196 (2007).
- 3) K. Ueno, S. Nakamura, H. Shimotani, A. Ohtomo, N. Kimura, T. Nojima, H. Aoki, Y. Iwasa, and M. Kawasaki, *Nat. Mater.* **7**, 855 (2008).
- 4) J. Biscaras, N. Bergeal, A. Kushwaha, T. Wolf, A. Rastogi, R. C. Budhani, and J. Lesueur, *Nat. Commun.* **1**, 89 (2010).
- 5) Y. Kozuka, M. Kim, C. Bell, B. G. Kim, Y. Hikita, and H. Y. Hwang, *Nature* **462**, 487 (2009).
- 6) K. Ueno, H. Shimotani, H. Yuan, J. Ye, M. Kawasaki, and Y. Iwasa, *J. Phys. Soc. Jpn.* **83**, 032001 (2014).
- 7) A. D. Caviglia, S. Gariglio, N. Reyren, D. Jaccard, T. Schneider, M. Gabay, S. Thiel, G. Hammerl, J. Mannhart, and J. M. Triscone, *Nature* **456**, 624 (2008).
- 8) C. Bell, S. Harashima, Y. Kozuka, M. Kim, B. G. Kim, Y. Hikita, and H. Y. Hwang, *Phys. Rev. Lett.* **103**, 226802 (2009).
- 9) M. Ben Shalom, M. Sachs, D. Rakhmilevitch, A. Palevski, and Y. Dagan, *Phys. Rev. Lett.* **104**, 126802 (2010).
- 10) A. D. Caviglia, M. Gabay, S. Gariglio, N. Reyren, C. Cancellieri, and J. M. Triscone, *Phys. Rev. Lett.* **104**, 126803 (2010).
- 11) P. Fulde and R. A. Ferrell, *Phys. Rev.* **135**, A550 (1964).
- 12) A. I. Larkin and Y. N. Ovchinnikov, *Zh. Eksp. Teor. Fiz.* **47**, 1136 (1964).

- 13) Y. Matsuda and H. Shimahara, J. Phys. Soc. Jpn. **76**, 051005 (2007).
- 14) J. Bardeen, L. N. Cooper, and J. R. Schrieffer, Phys. Rev. **108**, 1175 (1957).
- 15) A. Bianchi, R. Movshovich, C. Capan, P. G. Pagliuso, and J. L. Sarrao, Phys. Rev. Lett. **91**, 187004 (2003).
- 16) M. Kenzelmann, T. Strässle, C. Niedermayer, M. Sigrist, B. Padmanabhan, M. Zolliker, A. D. Bianchi, R. Movshovich, E. D. Bauer, J. L. Sarrao, and J. D. Thompson, Science **321**, 1652 (2008); M. Kenzelmann, S. Gerber, N. Egetenmeyer, J. L. Gavilano, T. Strässle, A. D. Bianchi, E. Ressouche, R. Movshovich, E. D. Bauer, J. L. Sarrao, and J. D. Thompson, Phys. Rev. Lett. **104**, 127001 (2010).
- 17) S. Uji, T. Terashima, M. Nishimura, Y. Takahide, T. Konoike, K. Enomoto, H. Cui, H. Kobayashi, A. Kobayashi, H. Tanaka, M. Tokumoto, E. S. Choi, T. Tokumoto, D. Graf, and J. S. Brooks, Phys. Rev. Lett. **97**, 157001 (2006).
- 18) R. Lortz, Y. Wang, A. Demuer, P. H. M. Böttger, B. Bergk, G. Zwicknagl, Y. Nakazawa, and J. Wosnitza, Phys. Rev. Lett. **99**, 187002 (2007).
- 19) B. Bergk, A. Demuer, I. Sheikin, Y. Wang, J. Wosnitza, Y. Nakazawa, and R. Lortz, Phys. Rev. B **83**, 064506 (2011).
- 20) H. Mayaffre, S. Kramer, M. Horvatić, C. Berthier, K. Miyagawa, K. Kanoda, and V. F. Mitrović, Nat. Phys. **10**, 928 (2014).
- 21) T. Terashima, K. Kihou, M. Tomita, S. Tsuchiya, N. Kikugawa, S. Ishida, C.-H. Lee, A. Iyo, H. Eisaki, and S. Uji, Phys. Rev. B **87**, 184513 (2013).
- 22) P. Burger, F. Hardy, D. Aoki, A. E. Böhmer, R. Eder, R. Heid, T. Wolf, P. Schweiss, R. Fromknecht, M. J. Jackson, C. Paulsen, and C. Meingast, Phys. Rev. B **88**, 014517 (2013).
- 23) D. A. Zocco, K. Grube, F. Eilers, T. Wolf, and H. v. Löhneysen, Phys. Rev. Lett. **111**, 057007 (2013).
- 24) Y.-a. Liao, A. S. C. Rittner, T. Paprotta, W. Li, G. B. Partridge, R. G. Hulet, S. K. Baur, and E. J. Mueller, Nature **467**, 567 (2010).
- 25) R. Casalbuoni and G. Nardulli, Rev. Mod. Phys. **76**, 263 (2004).
- 26) L. W. Gruenberg and L. Gunther, Phys. Rev. Lett. **16**, 996 (1966).
- 27) H. Adachi and R. Ikeda, Phys. Rev. B **68**, 184510 (2003).
- 28) H. Shimahara, J. Phys. Soc. Jpn. **67**, 736 (1998).
- 29) *Non-Centrosymmetric Superconductors: Introduction and Overview (Lecture Notes in Physics)*, ed. E. Bauer and M. Sigrist (Springer, Berlin/Heidelberg, 2012).
- 30) V. M. Edelstein, Sov. Phys. JETP **68**, 1244 (1989).
- 31) O. V. Dimitrova and M. V. Feigel'man, JETP Lett. **78**, 637 (2003).
- 32) K. V. Samokhin, Phys. Rev. B **70**, 104521 (2004).
- 33) R. P. Kaur, D. F. Agterberg, and M. Sigrist, Phys. Rev. Lett. **94**, 137002 (2005).
- 34) D. F. Agterberg and R. P. Kaur, Phys. Rev. B **75**, 064511 (2007).
- 35) O. Dimitrova and M. V. Feigel'man, Phys. Rev. B **76**, 014522 (2007).
- 36) K. Michaeli, A. C. Potter, and P. A. Lee, Phys. Rev. Lett. **108**, 117003 (2012).
- 37) A. Brinkman, M. Huijben, M. van Zalk, J. Huijben, U. Zeitler, J. C. Maan, W. G. van der Wiel, G. Rijnders, D. H. A. Blank, and H. Hilgenkamp, Nat. Mater. **6**, 493 (2007).
- 38) D. A. Dikin, M. Mehta, C. W. Bark, C. M. Folkman, C. B. Eom, and V. Chandrasekhar, Phys. Rev. Lett. **107**, 056802 (2011).
- 39) L. Li, C. Richter, J. Mannhart, and R. C. Ashoori, Nat. Phys. **7**, 762 (2011).
- 40) J. A. Bert, B. Kalisky, C. Bell, M. Kim, Y. Hikita, H. Y. Hwang, and K. A. Moler, Nat. Phys. **7**, 767 (2011).
- 41) Ariando, X. Wang, G. Baskaran, Z. Q. Liu, J. Huijben, J. B. Yi, A. Annadi, A. Roy Barman, A. Rusydi, S. Dhar, Y. P. Feng, J. Ding, H. Hilgenkamp, and T. Venkatesan, Nat. Commun. **2**, 188 (2011).
- 42) Y. Nakamura and Y. Yanase, J. Phys. Soc. Jpn. **82**, 083705 (2013).
- 43) A. Gurevich, Phys. Rev. B **82**, 184504 (2010).
- 44) A. Ptok and D. Crivelli, J. Low. Temp. Phys. **172**, 226 (2013).
- 45) T. Mizushima, M. Takahashi, and K. Machida, J. Phys. Soc. Jpn. **83**, 023703 (2014).
- 46) Y. Yanase and M. Sigrist, J. Phys. Soc. Jpn. **77**, 124711 (2008); See also Y. Yanase and S. Fujimoto, *Non-Centrosymmetric Superconductors: Introduction and Overview (Lecture Notes in Physics)*, ed. E. Bauer and M. Sigrist (Springer, Berlin/Heidelberg, 2012), Chap. 6.
- 47) A. F. Santander-Syro, O. Copie, T. Kondo, F. Fortuna, S. Pailhès, R. Weht, X. G. Qiu, F. Bertran, A. Nicolaou, A. Taleb-Ibrahimi, P. Le Fèvre, G. Herranz, M. Bibes, N. Reyren, Y. Apertet, P. Lecoeur, A. Barthélémy, and M. J. Rozenberg, Nature **469**, 189 (2011).
- 48) A. Joshua, S. Pecker, J. Ruhman, E. Altman, and S. Ilani, Nat. Commun. **3**, 1129 (2012).
- 49) G. Berner, M. Sing, H. Fujiwara, A. Yasui, Y. Saitoh, A. Yamasaki, Y. Nishitani, A. Sekiyama, N. Pavlenko, T. Kopp, C. Richter, J. Mannhart, S. Suga, and R. Claessen, Phys. Rev. Lett. **110**, 247601 (2013).
- 50) P. D. C. King, S. McKeown Walker, A. Tamai, A. de la Torre, T. Eknapakul, P. Buaphet, S.-K. Mo, W. Meevasana, M. S. Bahramy, F. Baumberger, Nat. Commun. **5**, 3414 (2014).
- 51) R. Pentcheva and W. E. Pickett, Phys. Rev. B **78**, 205106 (2008).
- 52) Z. S. Popović, S. Satpathy, and R. M. Martin, Phys. Rev. Lett. **101**, 256801 (2008).
- 53) P. Delugas, A. Filippetti, V. Fiorentini, D. I. Bilc, D. Fontaine, and P. Ghosez, Phys. Rev. Lett. **106**, 166807 (2011).
- 54) G. Khalsa and A. H. MacDonald, Phys. Rev. B **86**, 125121 (2012).
- 55) M. Hirayama, T. Miyake, and M. Imada, J. Phys. Soc. Jpn. **81**, 084708 (2012).
- 56) Z. Zhong, A. Tóth, and K. Held, Phys. Rev. B **87**, 161102 (2013).
- 57) G. Khalsa, B. Lee, and A. H. MacDonald, Phys. Rev. B **88**, 041302(R) (2013).
- 58) Y. Yanase, J. Phys. Soc. Jpn. **82**, 044711 (2013).
- 59) J. A. Bert, K. C. Nowack, B. Kalisky, H. Noad, J. R. Kirtley, C. Bell, H. K. Sato, M. Hosoda, Y. Hikita, H. Y. Hwang, and K. A. Moler, Phys. Rev. B **86**, 060503(R) (2012).
- 60) S. N. Klimin, J. Tempere, J. T. Devreese, and D. van der Marel, Phys. Rev. B **89**, 184514 (2014).
- 61) J. F. Schooley, W. R. Hosler, and M. L. Cohen, Phys. Rev. Lett. **12**, 474 (1964).
- 62) Y. Nakamura and Y. Yanase, JPS Conf. Proc. **3**, 015027 (2014).
- 63) Y. Yanase and M. Sigrist, J. Phys. Soc. Jpn. **76**, 124709 (2007).
- 64) If the induced p -wave component in the order parameter is comparable to the s -wave component, a multigap structure should appear in the superconducting state. However, the multigap structure has not been observed in the SrTiO₃/LaAlO₃ interface.⁵⁹⁾
- 65) K. Yada, S. Onari, Y. Tanaka, and J. Inoue, Phys. Rev. B **80**, 140509 (2009).
- 66) M. S. Scheurer and J. Schmalian, arXiv:1404.4039.
- 67) V. L. Berezinskii, Sov. Phys. JETP **32**, 493 (1971) [Zh. Eksp. Theor. Fiz. **59**, 907 (1970)].
- 68) J. M. Kosterlitz and D. J. Thouless, J. Phys. C **6**, 1181 (1973).
- 69) H. Shimahara, J. Phys. Soc. Jpn. **67**, 1872 (1998).
- 70) T. Schneider, A. D. Caviglia, S. Gariglio, N. Reyren, and J.-M. Triscone, Phys. Rev. B **79**, 184502 (2009).
- 71) E. I. Rashba, Sov. Phys. Solid State **1**, 368 (1959).
- 72) T. Yoshida, M. Sigrist, and Y. Yanase, J. Phys. Soc. Jpn. **82**, 074714 (2013).
- 73) D. F. Agterberg, E. Babaev, and J. Garaud, Phys. Rev. B **90**, 064509 (2014). The authors investigated the vortex structure in the single-band CS state at low temperatures. We can conclude that the skyrmion lattice is stabilized in the ODCS phase near $T = T_c$ because of the repulsive interaction between two-component order parameters when $-\beta < \gamma < 0$.